Matching between the electron candidate track and the Cherenkov counter hit

M. Osipenko[a,b], A. Vlassov[c], M. Taiuti[d]

[a] INFN, sez. di Genova, 16146 Genova, Italy
[b] Moscow State University, 119992 Moscow, Russia
[c] Institute for Theoretical and Experimental Physics, Moscow, Russia 117259
[d] Università di Genova, 16146 Genova, Italy

June 18, 2004

0.1 Introduction

The Cherenkov Counter (CC) installed in the CLAS detector aimed to separate scattered electrons from a background of negatively charged pions. These pions are mainly produced in quasi-real photoproduction i.e. when scattered electron goes at polar angle θ very close to zero and therefore not measured by CLAS. According to the original design, CC is very efficient in the Cherenkov light detection. As it was shown in numerous analyses e.g. Ref. [3], within specially defined "fiducial" regions of CLAS acceptance, CC inefficiency does not exceed 2%. In the same time, the electron-pion separation does not work at the same level of precision and some pion contamination shows up in an electron candidate sample. This is especially important at the highest JLab beam energies, where the rate of low momenta pions is very significant. Therefore, the main goal of our analysis is to reduce the pion contamination as much as possible by means of a better event reconstruction.

An example of the photo-electron distribution as measured in CC is shown in Fig. 1 for a few values of beam energy and torus magnetic field. From Fig. 1 it is clear that the peak at single photo-electron (we call single photo-electron peak the peak which is actually located at 1-2 photo-electrons) is not expected to be produced by electrons crossing CC within its fiducial volume. In fact, in the energy fraction $ECtot/P$ of the electron candidate sample, the single photo-electron peak events (see low region in Fig. 2) have much smaller mean released energy fraction than expected for electrons. Therefore, we can conclude that the single photo-electron peak is produced by the tail of minimum ionizing particles - negatively charged pions.

The fixed position of this peak at about one photo-electron, independently on the kinematics under study, indicates that this CC signal is originated from the PMT internal noise. CLAS electron run trigger requires a coincidence of the charged particle track measured in DC with hits in EC and CC above some certain threshold within the time window of 150 ns. The matching between the sector where the track was measured in DC and the sector where hits in EC and CC were detected was requested. Meantime, within one sector no geometrical matching between the track and CC hit was applied. Thus, a coincidence of the pion track in DC with CC noise signal not related to the track, but located within the same CLAS sector is possible. In fact, such events can be easily seen in the reconstructed data e.g. in Fig. 3.

CLAS sector consists of 18 CC segments each containing two PMTs, therefore the probability to have the coincidence is a product of probabilities to have the noise hit in the one of 36 PMTs together with negative pion track within $\delta t = 150$ ns time interval. The average CC PMT noise rate R^{PMT} in CLAS was measured and found to be ≈ 42 kHz. In order to estimate electron and pion rates we measured them in the conditions (a set of cuts) applied for a normal electron identification. That includes cuts on the fraction of energy released in EC, status word cut and kinematic fiducial cuts. For the typical running conditions of E6 (I=10 nA, $\rho x = 0.65$ LD), within fiducial cuts, average rate of negatively charged hadrons having appropriate EC signal ($ECtot/P > 0.2$) is of the order
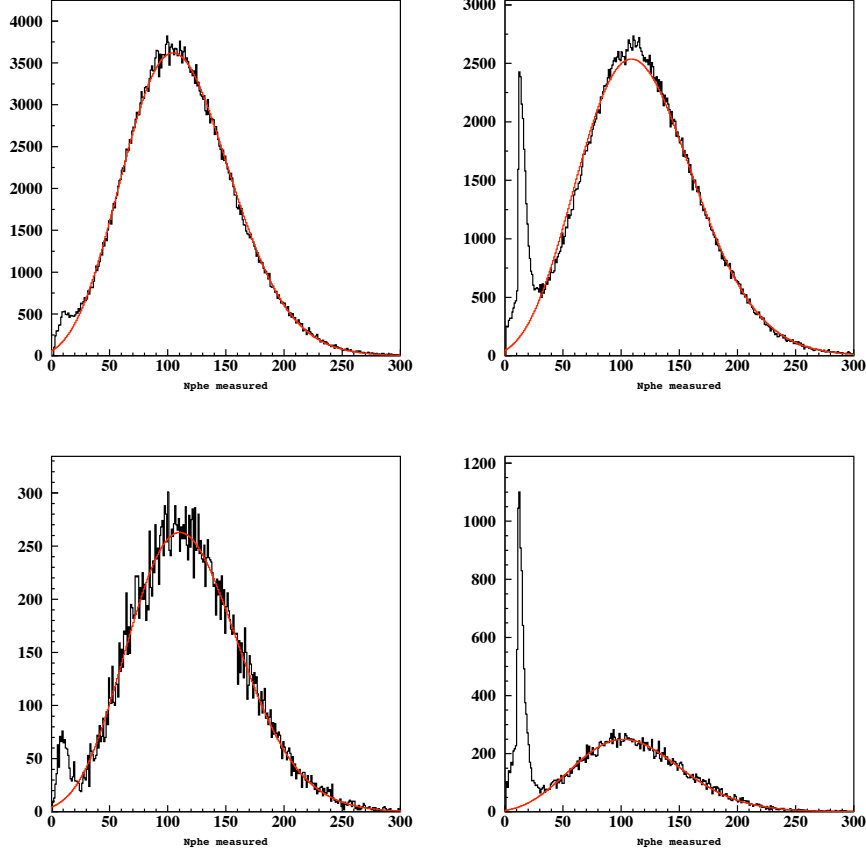
2

Figure 1: Measured number of photoelectrons (multiplied by 10) in CC within fiducial cuts in comparison with expected from ep elastic data parameterization (red curve). Run E1d, E=2.474 GeV torus current 1500 A (left) run E6a E=5.77 GeV torus current 2250 A (right) in CC segment 8 (top) and 16 (bottom) of sector 1.

of $R^{h-} \approx 2.3$ kHz. This gives an estimate of possible contamination:

$$R^{1phe} = R^{PMT} R^{h-} \delta t \approx 15 \text{ Hz} \quad , \tag{1}$$

which has to be compared to the electron rate R^{e-}, defined within the same cuts condition and found to be ≈ 250 Hz. Therefore, the expected contamination is of the order of 6% overall. In contrast for small momenta $p < 1$ GeV and large scattering angle $\theta > 30°$ we get $R^{h-} \approx 1.7$ kHz and $R^{e-} \approx 100$ Hz resulting in the contamination α of 12% calculated as follows:

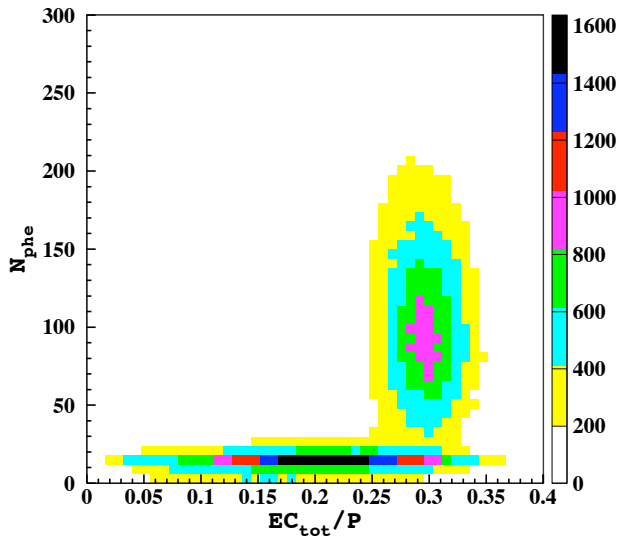$$\alpha = \frac{R^{1phe}/R^{e-}}{1 - R^{1phe}/R^{e-}} \tag{2}$$

Figure 2: Number of photo-electrons (multiplied by 10) measured in CC vs. energy fraction released in EC for electron candidate sample.

The estimated contamination cannot be easily removed from electron candidate sample because both shapes of single photo-electron peak and peak of real electrons are not known. In fact the parameterized photo-electron distributions shown by red line in Fig. 1 reproduce experimental spectra only in a few particular cases. Moreover, it has to be adjusted for each particular run period accounting for possible PMT gain changes. The procedure helping to reduce the background of these coincidences is described in the following section.
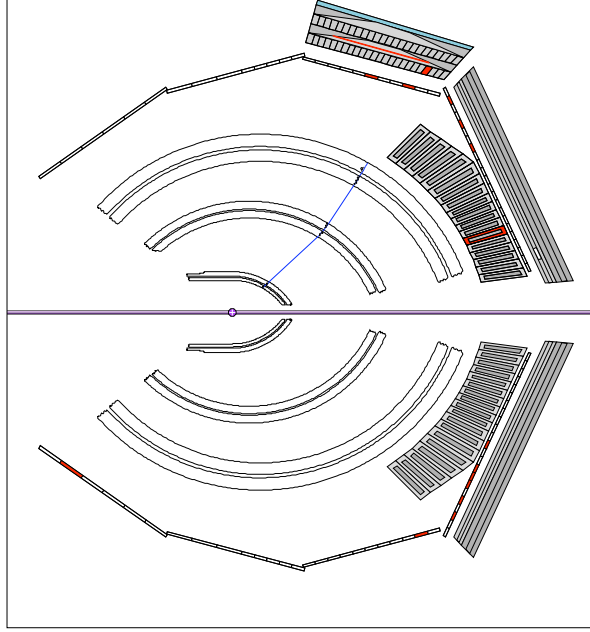
Figure 3: Example of charged particle track in coincidence with CC noise hit in CLAS; the track is drawn by blue line and CC hit is indicated by red color far away from the track.

0.2   Matching between CC hit and the track

In order to strongly reduce the contamination of hadron track - accidental CC hit coincidences we propose to apply geometrical and temporal matching between CC hit and the measured track. This procedure was done in the following way:

1. we defined CC projective plane which represents an imaginary plane behind the CC detector where Cherenkov radiation would arrive in the case it propagated the same distance from emission point to PMT but doing no reflections in the mirror system (see Fig. 4). This plane can be defined [3] in the sector reference coordinate system as follows:

$$1 - 7.840784063 \times 10^{-4}x - 1.681461571 \times 10^{-3}z = 0 \qquad (3)$$

2. for each CC segment we found the polar angle from the CLAS center to the image of CC segment center and its edges in CC projective plane;

3. then the impact point and the direction in SC plane, as measured in DC, of the track were used to obtain the measured polar angle θ_p in projective plane for each electron candidate event (e.g. Fig. 5). Some shifts θ_p^{offset} in the segment center position were observed (see Fig. 5) and taken into account in the further calculations. Although the

width of the distributions turns out to be compatible with known from geometrical configuration (see th_delt in CCG bank), we fitted the θ_p distributions separately for each CC segment in order to extract their measured width σ_p;

4. for each CC segment we applied a cut

$$|\theta_p - \theta_p^{center} - \theta_p^{offset}| < 3\sigma_p \qquad (4)$$

which was aimed to remove those electron event candidates which had the track impact point in CC far away from the segment where hit was detected. In Fig. 5 an example of the θ_p distribution is shown for one segment and the cut applied is indicated by green lines. To clearly identify the contribution of the coincidences and check our cut we separated events in the single photo-electron peak from the others applying a cut $N_{phe} > 2.5$. This is shown in Fig. 5 by different colors: red histogram shows events in the single photo-electron peak, while blue histogram represents events with $N_{phe} > 2.5$ photo-electron. One can clearly see that single photo-electron peak events produced tails in θ_p range much larger that the main peak width. However, some coincidence events are present also in the blue histogram. This means that $N_{phe} > 2.5$ cut is not sufficient to remove all the coincidence background.

5. to perform time matching between CC and SC hits of the electron candidate event we first calibrated time-offsets of CC signal with respect to SC (CC timings are not calibrated). For this purpose for each CC segment we measured Δt^{SC-CC} defined as following:

$$\Delta t^{SC-CC} = t^{SC} - t^{CC} - \frac{r^{SC} - r^{CC}}{c\beta} \qquad (5)$$

The distribution of SC-CC time-offsets is shown in Fig. 6 separately for events in the single photo-electron peak and for events above 2.5 photo-electrons. Since we observed some additional structure at the r.h.s. of the main peak corresponding to "good" electron candidates we performed only a cut of the left part of the distribution as shown in Fig. 6 by the green line. There are two features of the Δt^{SC-CC} distributions which have to be discussed. The first one is related to the presence of two peaks located close one to another. This can be explained by some time offset of two PMTs of CC segment. In fact if one plot the Δt^{SC-CC} distribution separately for each PMT in CC segment as it shown in Fig. 7 it becomes clear that two PMTs are a little bit offset by a small time interval. Another issue is concerns the structure at about 60 ns in Δt^{SC-CC} distribution. We checked which timing signal is responsible for this structure. In Fig. 8 we plotted Δt^{EC-CC} and Δt^{EC-SC} distributions for the same CC segment. As one can see the structure is still present in Δt^{EC-CC} distribution while Δt^{EC-SC} distribution has only one main peak. This

6

allowed us to conclude that the spurious structure at 60 ns in Δt^{SC-CC} is related to CC timing.

6. The measured photo-electron distribution for the electron candidate events was compared to the one after all the cuts described above had been applied. This is shown by different colors in Fig. 9.
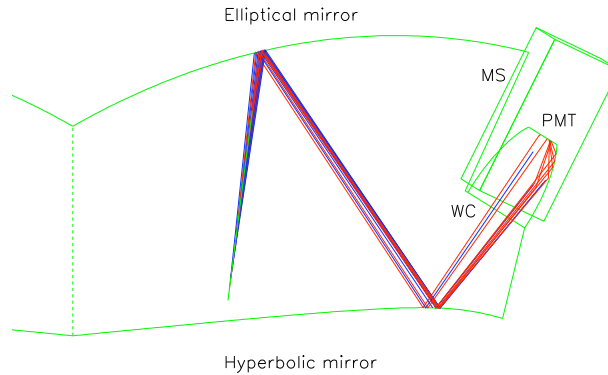

Figure 4: Cherenkov light tracing in CC mirror system. Projective plane can be defined by Cherenkov light rays (red lines) propagating the distance from emission point to PMT along the straight line of the initial radiation direction.

In order to estimate the contamination we used the same method as in Ref. [6]. This method represents a fitting procedure of the photo-electron spectra with two Poisson distributions convoluted with a Gaussian as shown in Fig. 10. Then the ratio between electron peak area (red area in Fig. 10) over the total one give the value of the necessary correction to the data as a function of scattered electron angle and momentum. An example of the fit before and after the CC matching is shown in Fig. 11.
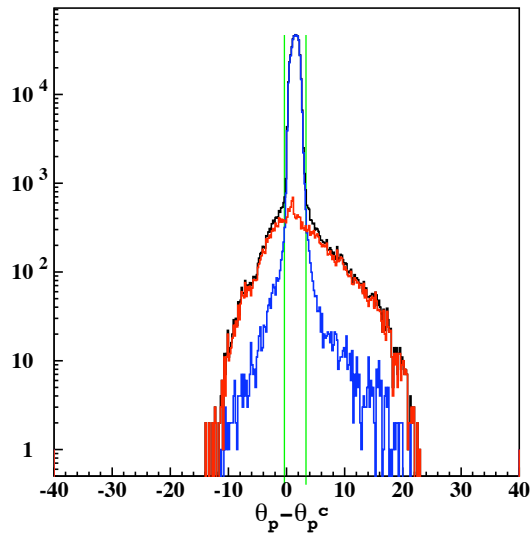
Figure 5: Difference between the measured angle θ_p in CC projective plane and segment center position for electron event candidates in single photo-electron peak (red) and those having number of photo-electrons above 2.5 (blue); the cut applied to the data is shown by green lines.
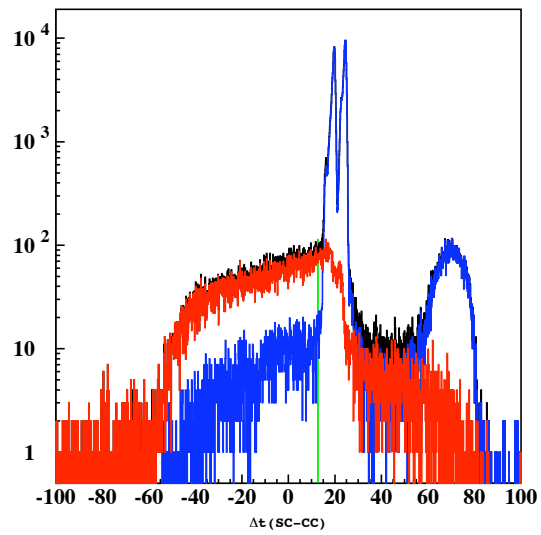
Figure 6: Measured time offset Δt between SC and CC hits for electron event candidates in single photo-electron peak (red) and those having number of photo-electrons above 2.5 (blue); the cut applied to the data is shown by green line.
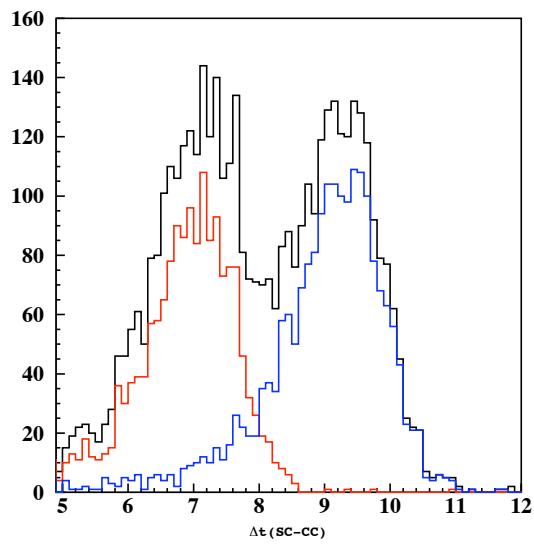
Figure 7: Measured time offset Δt between SC and CC hits for electron event candidates in one CC segment (black) separately for each PMT of the CC segment: left PMT (red) and right PMT (blue).
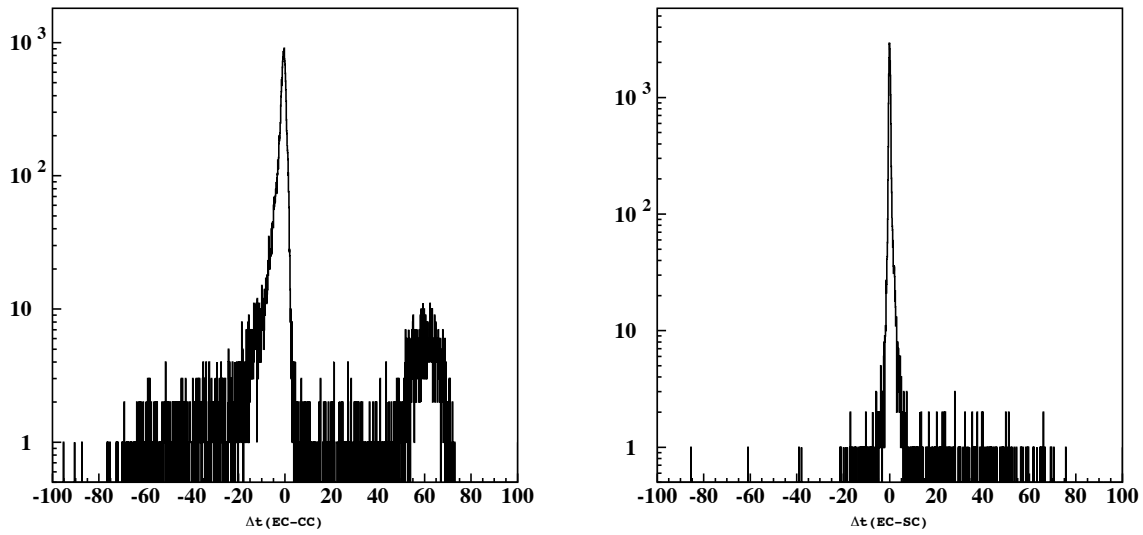
Figure 8: Measured time offset Δt between EC and CC hits (left) and between EC and SC hits (right) for electron event candidates. The structure at 60 ns is only present in CC timing.
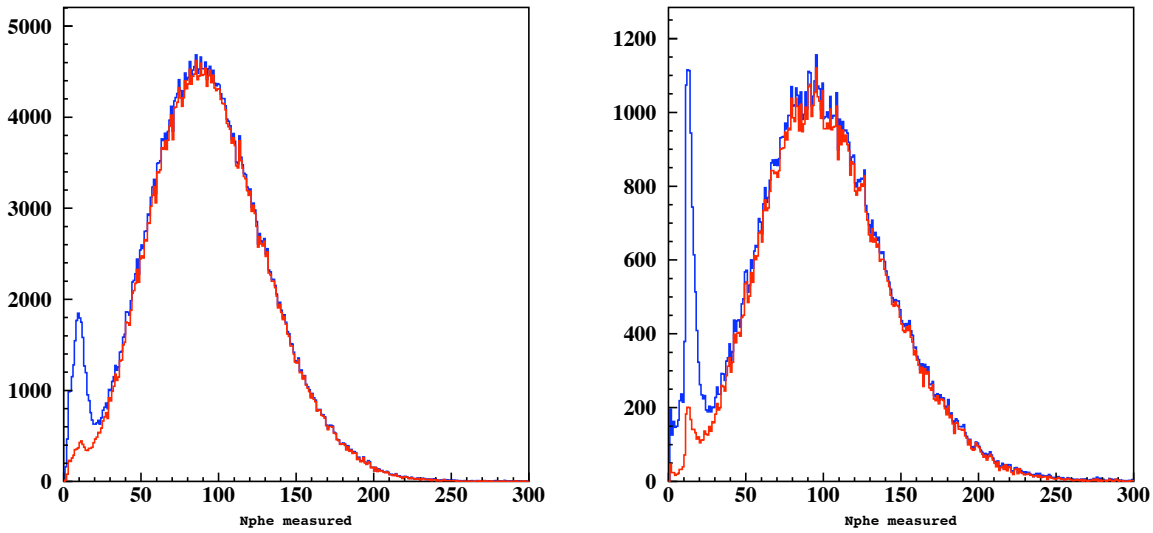
11

Figure 9: Number of photo-electrons measured in CC for electron event candidates before (blue) and after (red) cut on the geometrical and temporal matching of CC hit with DC track and time measured in SC in sector 4, segment 9 for E1d run period E=2.474 GeV 1500 A (left) and E6a run period E=5.77 GeV I=2250 A (right).
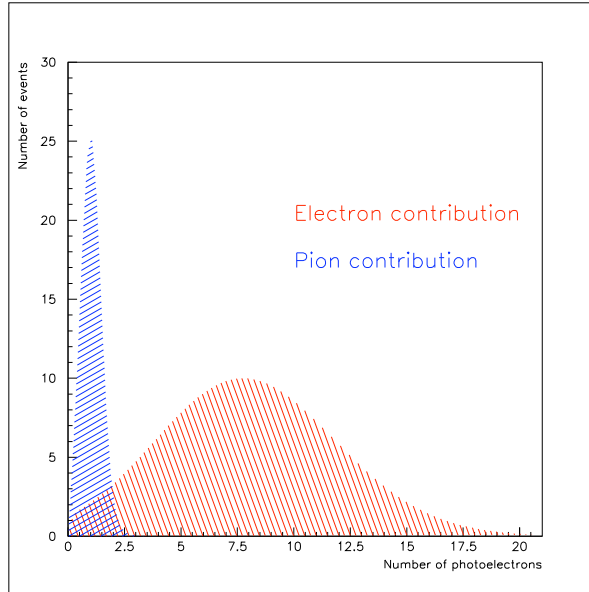

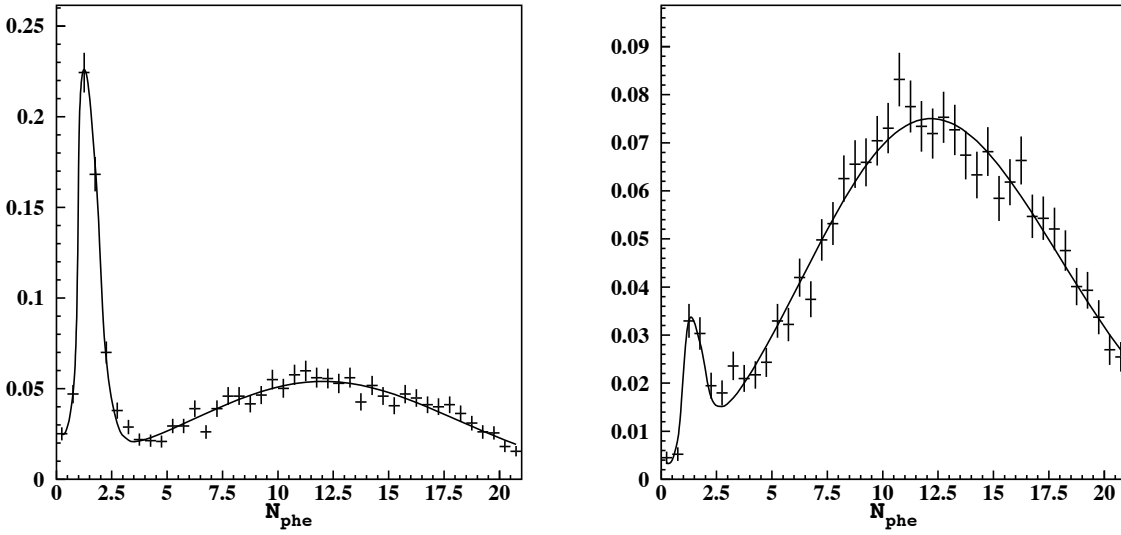Figure 10: Electron-pion separation in the measured in CC photo-electron distribution.

12

Figure 11: Fit of normalized photo-electron distributions with two Poissonians convoluted with a Gaussian for E6a E=5.77 GeV I=2250 A, sector 2, $\theta = 38 - 40°$ before (left) and after (right) CC matching procedure.

0.3 Conclusions

The contamination in the electron candidate sample measured in CLAS appearing as a single photoelectron peak in the measured CC spectra is explained. The main source of this contamination is the coincidence of accidental PMT noise signal in one of 36 PMTs in the CLAS sector with measured pion track produced mainly in quasi-real electroproduction, when electron is going at very small polar angles to the forward hole of CLAS. This coincidence takes place due to lack of matching between CC hit and the track within one sector of CLAS. A procedure of geometrical and temporal matching between CC hit with track in DC and time of flight measured in SC was developed. The procedure is shown to be very efficient to remove background events (see Fig. 9). An example of the contamination reduction as a function of electron momentum P is shown in Fig. 12: black points represent a fraction of real electrons in the electron candidate sample extracted applying normal electron identification cuts ($ECtot/P > 0.2$ and event status equal to 4), the red points are obtained from the same data applying the CC matching procedure described above. The pion contamination reduces from 30% to 5% in the worst case. The remaining contamination is due to those events where the pion track coincide with an accidental PMT noise signal in the same CC segment crossed by the track. The fraction of such events is expected to be 1/18 from the total number of coincidences. Obtained reduction factor is about 6 which is three times smaller than expected one and probably related to loose cuts of the matching procedure.

Fortran code of the program is available and can be send on request.

We are gratefull to Dr. M. Anghinolfi for the usefull discussions and suggestions during preparation of this note.
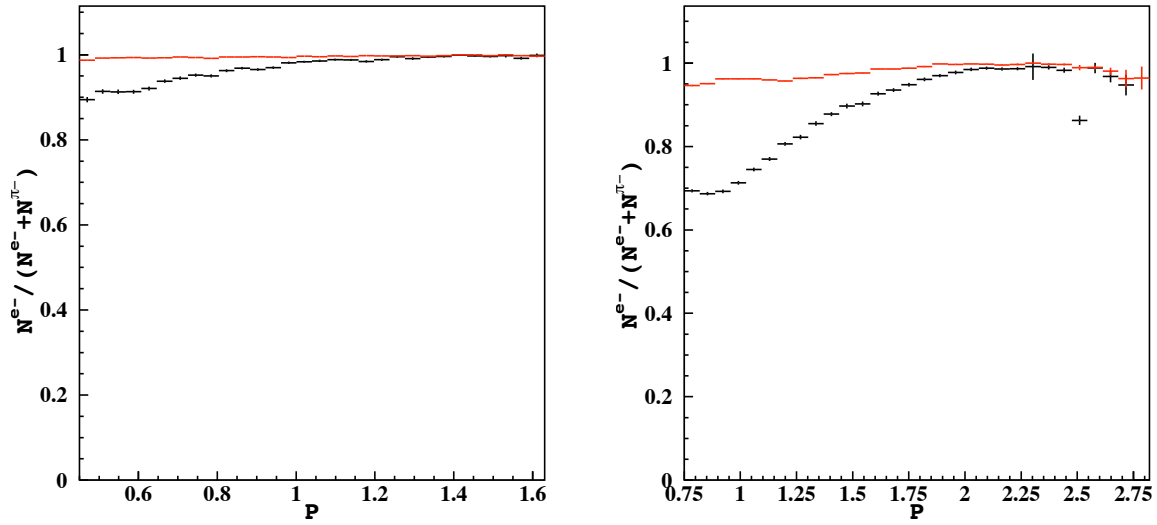
14

Figure 12: Ratio of the number of electrons over the sum of electrons and pions in electron candidate sample for sector 3 and $\theta = 27 - 29°$ for E1d run period E=2.474 GeV I=1500 A (left) and E6a E=5.77 GeV I=2250 A (right) before (black) and after (red) the CC matching procedure.

Bibliography

[1] M. D. Mestayer *et al.*, *Nucl. Instr. and Meth.* **A449**, 81 (2000).

[2] E. S. Smith *et al.*, *Nucl. Instr. and Meth.* **A432**, 265 (1999).

[3] G. Adams *et al.*, *Nucl. Instr. and Meth.* **A465**, 414 (2001).

[4] M. Amarian *et al.*, *Nucl. Instr. and Meth.* **A460**, 460 (2001).

[5] http://improv.unh.edu/Maurik/gsim_info.shtml.

[6] M. Osipenko *et al.*, Phys.Rev. **D67** 092001 (2003).